SPMSMs HFI Based Self-Sensing Using Intentional Magnetic Saturation

YE GU KANG[1]**, (Member, IEEE), DAVID DIAZ REIGOSA**[2]**, (Member, IEEE),
AND ROBERT D. LORENZ*, (Life Fellow, IEEE)**
[1]Mechanical Engineering Department, University of Wisconsin–Madison, Madison, WI 53705, USA
[2]Electrical Engineering Department, University of Oviedo, 33203 Gijon, Spain

Corresponding author: Ye Gu Kang (kangyegoo@gmail.com)

*Robert D. Lorenz is deceased.

ABSTRACT High-frequency injection (HFI) is widely used for zero-to-low speed self-sensing in machines with saliency. HFI algorithms use inductive saliency in the d- and q-axes to estimate the rotor position in permanent magnet synchronous machines (PMSMs). Generally speaking, surface PMSMs (SPMSMs), which are designed without inductive saliency, are not suitable for HFI inductive based self-sensing. In this article, a method to enhance HFI algorithms at zero-to-low speed for classically designed SPMSMs with low inductive saliency is presented. The proposed method is based on using intentional magnetic saturation under flux-intensifying (FI) operation, which will temporarily enable robust self-sensing operation in the zero-to-low speed region in machines that are not suitable for traditional HFI self-sensing.

INDEX TERMS High-frequency injection, magnetic saturation, permanent magnet, self-sensing, SPMSM.

NOMENCLATURE

SUPERSCRIPT

$\wedge$	Estimated variables.
$*$	Commanded variables.
θ_r	Rotor reference frame.
$\hat{\theta}_r$	Estimated rotor reference frame

SYMBOLS AND ABBREVIATIONS

λ_d, λ_q	D-, q-axes flux-linkages.
$\lambda_{dsHF}, \lambda_{qsHF}$	D-, q-axes high-frequency flux-linkages.
$\lambda_{\alpha HF}, \lambda_{\beta HF}$	Alpha-, beta-axes high-frequency flux-linkages.
λ_{PM}	PM flux-linkage.
ω_{HFI}	High-frequency injection frequency in rad/sec.
P_{HFI}	High-frequency injection loss.
P_{FI}	Flux-intnesifying operation loss.
P_{FIHFI}	Total loss during flux-intensifying high-frequency injection self-sensing operation.
p	Derivative operator.
i_d, i_q	D- and q-axes currents.
i_{dsHF}, i_{qsHF}	D- and q-axes high-frequency currents.

$i_{\alpha HF}, i_{\beta HF}$	Alpha- and beta-axes high-frequency currents.
I_{i0}, I_{i1}	Average and differential carrier currents.
I_{ch}	Characteristic current.
$L_{dd,qq}$	D- and q-axes inductances.
$L_{dq,qd}$	D- and q-axes cross-coupling inductances.
L_p, L_{uv}	Phase and phase-to-phase inductances.
$\Delta L, \Sigma L$	Differential and average inductances.
θ_{HFI}	High-frequency injection angles.
f_{HFI}	High-frequncy injection freuqnecy in Hz.
R_p	Phase resistance.
ε	Injection angle error.
V_{HFI}	High-frequency injection voltage.
FI	Permanent magnet flux-intensifying operation.
FW	Permanent magnet flux-weakening operation.

I. INTRODUCTION

High-frequency injection (HFI) is a self-sensing technique widely used in machines with inductive saliency in the zero-to-low speed operational region [1]. Since surface permanent magnet synchronous machine (SPMSM) rotor geometry is symmetrical, no inductive saliency exists based on

the machine's rotor geometry. SPMSM is therefore not considered a suitable machine for HFI based self-sensing. To improve the use of HFI techniques in SPMSMs, research efforts have been focused on increasing the signal-to-noise ratio (SNR) [2]–[4], and increasing inductive saliency by modifying the design of SPMSMs [5]–[8].

Saturation and cross-saturation effects and self-sensing control strategies have been investigated in depth for interior permanent magnet synchronous machines (IPMSMs). In [9]–[12] inductance ellipse variation under load condition is analyzed for IPMSMs. Orientation and eccentricity of the inductance ellipse have been shown to vary depending on the dq-axes current level; the orientation of the ellipse has been shown to depend on the cross saturation, while the eccentricity of the ellipse has been shown to depend on the inductive saliency between d- and q-axes. In [10], self-sensing performance is improved by decoupling the cross-saturation effect under loaded conditions. In [11], [12], HF is injected in tilted phase angle to improve the self-sensing performance of an IPMSM while operating the machine near the maximum torque per ampere (MTPA) trajectory. In [9]–[12], additional efforts based on offline characterization of saturation and cross-saturation have been made to enhance the self-sensing performance of PMSMs.

For the case of SPMSMs, large HF injection voltages have been proposed to be used, which results in changes in d-axis impedance based on magnetic saturation effect[13]. SPMSMs operation in MTPA trajectory did not affect the self-sensing ability [14], [15]. In [15], control algorithm to enable non-salient SPMSM using d-axis current planning is investigated with stationary reference frame HF injection. However, the optimal HF injection phase angle for SPMSMs has not been investigated. In [16], the variation of inductive saliency of a SPMSM under loaded conditions is experimentally investigated. Nevertheless, generalization of the use of intentional magnetic saturation induced inductive saliency has not been made.

This article proposes a novel technique based on intentional magnetic saturation with PM flux-intensifying (FI) current, i.e., positive fundamental d-axis current, $+ i_d$, injection, on SPMSMs. The physics-based model with variable inductance is developed from the machine design perspective of view considering characteristic current, I_{ch}, offset biasing on d-axis flux path. The generalized SPMSM magnetic saturation characteristic model and analysis are supported by Finite Element Analysis (FEA) and machine characterization experimental results. The proposed technique utilizes positive fundamental d-axis current injection to intentionally increase the inductive saliency; making reliable use of classical HFI self-sensing techniques in machines with very low saliency, e.g., SPMSMs. FI operation with positive d-axis current in the estimated rotor reference frame will results in a decrease of d-axis incremental inductance which results in an increased inductive saliency; therefore, saliency-based self-sensing ability will be enhanced [17]. No pre-characterization of SPMSM nor complex saturation,

cross-saturation compensation techniques are required considering the main flux path saturation effect on d-axis which is the dominant factor of SPMSM self-sensing. The increasing self-sensing sensitivity is verified experimentally, using decoupled differential current, I_{i1} [18].

The article is organized as follows: Section II presents basics of HFI based self-sensing control, Section III presents the concept of FI operation using intentional magnetic saturation; Section IV presents simulation results of the proposed self-sensing technique using intentional magnetic saturation; Section V discusses implementation issues of the proposed technique; Section VI shows experimental results to demonstrate the viability of the proposed technique; Finally, the conclusions of the article are presented in Section VII.

II. HFI BASED SELF-SENSING CONTROL CONSIDERING MAGNETIC SATURATION EFFECT

This section shows the PM machine model used for HFI based self-sensing. The flux-linkage model of a PMSM in a reference frame synchronous with the rotor is shown in (1), where ΔL, ΣL are the differential and average inductances, (2) and (3), respectively, L_{dd} and L_{qq} are the d- and q-axes incremental inductances which are function of dq-current [10], [13], [14], [19]. $\lambda_{dsHF}^{\theta_r}$, $\lambda_{qsHF}^{\theta_r}$, $i_{dsHF}^{\theta_r}$, and $i_{qsHF}^{\theta_r}$ are the d- and q-axes stator flux-linkages and stator currents in a reference frame synchronous with the rotor.

$$\begin{bmatrix} \lambda_{dsHF}^{\theta_r} \\ \lambda_{qsHF}^{\theta_r} \end{bmatrix} = \begin{bmatrix} \Sigma L - \Delta L & 0 \\ 0 & \Sigma L + \Delta L \end{bmatrix} \begin{bmatrix} i_{dsHF}^{\theta_r} \\ i_{qsHF}^{\theta_r} \end{bmatrix} \tag{1}$$

$$\Delta L\{i_d, i_q\} = \frac{1}{2}(L_{qq}\{i_d, i_q\} - L_{dd}\{i_d, i_q\}) \tag{2}$$

$$\Sigma L\{i_d, i_q\} = \frac{1}{2}(L_{qq}\{i_d, i_q\} + L_{dd}\{i_d, i_q\}) \tag{3}$$

$$K_p(\varphi) = \begin{bmatrix} \cos(\varphi) & \sin(\varphi) \\ -\sin(\varphi) & \cos(\varphi) \end{bmatrix} \tag{4}$$

$$\begin{aligned} \begin{bmatrix} \lambda_{\alpha HF} \\ \lambda_{\beta HF} \end{bmatrix} &= K_p^{-1} \begin{bmatrix} \lambda_{dsHF}^{\theta_r} \\ \lambda_{qsHF}^{\theta_r} \end{bmatrix} \\ &= \left\{ K_p^{-1}(\theta_r) \begin{bmatrix} \Sigma L - \Delta L & 0 \\ 0 & \Sigma L + \Delta L \end{bmatrix} K_p(\theta_r) \right\} \\ &\quad \times K_p^{-1}(\theta_r) \begin{bmatrix} i_{dsHF}^{\theta_r} \\ i_{qsHF}^{\theta_r} \end{bmatrix} \\ &= \begin{bmatrix} \Sigma L - \Delta L \cos(2\theta_r) & -\Delta L \sin(2\theta_r) \\ -\Delta L \sin(2\theta_r) & \Sigma L + \Delta L \cos(2\theta_r) \end{bmatrix} \\ &\quad \times \begin{bmatrix} i_{\alpha HF} \\ i_{\beta HF} \end{bmatrix} \end{aligned} \tag{5}$$

Using the inverse of the Park transform (4), the dq-axes flux-linkage model can be transformed into the stator reference frame, i.e., stationary reference frame (5), where $\lambda_{\alpha HF}$, $\lambda_{\beta HF}$, $i_{\alpha HF}$, and $i_{\beta HF}$ are the alpha- and beta-axes stator flux-linkages and currents.

Pulsating HF voltage command is shown in the estimated rotor reference frame and in the stationary reference frame in (6) and (7) respectively, where θ_{HFI} is the high-frequency

injection angle (9), ω_{HFI} is the angular frequency of the high-frequency signal, V_{HFI} is the magnitude of the high-frequency signal, $\hat{\theta}_r$ is the estimated rotor position and

is the rotor position. When (7) is injected into the PMSM terminals, the resulting pulsating HF flux is (8), where $1/p$ represents an integrator. Substituting (8) into (10), the resulting HF currents in the stationary reference frame are represented by (11).

$$\begin{bmatrix} v_{dsHF}^{\hat{\theta}_r} \\ v_{qsHF}^{\hat{\theta}_r} \end{bmatrix} = V_{HFI}\cos(\theta_{HFI})\begin{bmatrix} 1 \\ 0 \end{bmatrix} \tag{6}$$

$$\begin{bmatrix} v_{\alpha HF} \\ v_{\beta HF} \end{bmatrix} = V_{HFI}\cos(\theta_{HFI})\begin{bmatrix} \cos(\hat{\theta}_r) \\ \sin(\hat{\theta}_r) \end{bmatrix} \tag{7}$$

$$\begin{bmatrix} \lambda_{\alpha HF} \\ \lambda_{\beta HF} \end{bmatrix} = \frac{1}{p}\begin{bmatrix} v_{\alpha HF} \\ v_{\beta HF} \end{bmatrix} = \frac{V_{HFI}\sin(\theta_{HFI})}{\omega_{HFI}}\begin{bmatrix} \cos(\hat{\theta}_r) \\ \sin(\hat{\theta}_r) \end{bmatrix} \tag{8}$$

$$\theta_{HFI} = \omega_{HFI}t \tag{9}$$

$$\begin{bmatrix} i_{\alpha HF} \\ i_{\beta HF} \end{bmatrix} = \begin{bmatrix} \Sigma L - \Delta L\cos(2\theta_r) & -\Delta L\sin(2\theta_r) \\ -\Delta L\sin(2\theta_r) & \Sigma L + \Delta L\cos(2\theta_r) \end{bmatrix}^{-1}$$
$$\times \begin{bmatrix} \lambda_{\alpha HF} \\ \lambda_{\beta HF} \end{bmatrix} \tag{10}$$

$$\begin{bmatrix} i_{\alpha HF} \\ i_{\beta HF} \end{bmatrix} = \frac{V_{HFI}\sin(\theta_{HFI})}{\omega_{HFI}\left(\Sigma L^2 - \Delta L^2\right)}$$
$$\times \begin{bmatrix} \Sigma L\cos(\hat{\theta}_r) + \Delta L\cos(2\theta_r - \hat{\theta}_r) \\ \Sigma L\sin(\hat{\theta}_r) + \Delta L\sin(2\theta_r - \hat{\theta}_r) \end{bmatrix} \tag{11}$$

By transforming (11) into the estimated rotor reference frame, (12), (13) is obtained.

$$K_p(\hat{\theta}_r)\begin{bmatrix} i_{\alpha HF} \\ i_{\beta HF} \end{bmatrix}$$
$$= K_p(\hat{\theta}_r)\begin{bmatrix} \Sigma L - \Delta L\cos(2\theta_r) & -\Delta L\sin(2\theta_r) \\ -\Delta L\sin(2\theta_r) & \Sigma L + \Delta L\cos(2\theta_r) \end{bmatrix}^{-1}$$
$$\times \begin{bmatrix} \lambda_{\alpha HF} \\ \lambda_{\beta HF} \end{bmatrix} \tag{12}$$

$$\begin{bmatrix} i_{dsHF}^{\hat{\theta}_r} \\ i_{qsHF}^{\hat{\theta}_r} \end{bmatrix}$$
$$= \frac{V_{HFI}\sin(\theta_{HFI})}{\omega_{HFI}\left(\Sigma L^2 - \Delta L^2\right)}\begin{bmatrix} \Sigma L + \Delta L\cos(2(\theta_r - \hat{\theta}_r)) \\ \Delta L\sin(2(\theta_r - \hat{\theta}_r)) \end{bmatrix} \tag{13}$$

The position estimation will be achieved by controlling the q-axis current in (13), $i_{qsHF}^{\hat{\theta}_r}$ (14), to zero; I_{i1} in (14) being the magnitude of the differential HF current (15). Note that (15) is a function of dq-current; it can be, therefore, concluded that the sensitivity of I_{i1} with respect to estimated position error, $(\theta_r - \hat{\theta}_r)$, depends on the operating condition. It can be concluded from (13)-(15) that without having ΔL, i.e., inductive saliency, HFI based self-sensing speed/position control cannot be performed. It will be shown in the next section that injecting positive d-axis current, flux intensifying (FI) current, will increase the inductive saliency (ΔL), making HFI based self-sensing techniques more reliable in machines

with low inductive saliency.

$$i_{qsHF}^{\hat{\theta}_r} = \sin(\theta_{HFI})I_{i1}\sin(2(\theta_r - \hat{\theta}_r)) \tag{14}$$

$$I_{i1}\{i_d, i_q\} = \frac{V_{HFI}}{\omega_{HFI}}\frac{\Delta L\{i_d, i_q\}}{\Sigma L\{i_d, i_q\}^2 - \Delta L\{i_d, i_q\}^2} \tag{15}$$

It is important to note that the nature of the inductive saliency-based self-sensing control does not require to know precise inductance values, unlike other model-based control algorithms, e.g., observer-based field-oriented control (FOC) [20] or deadbeat direct torque and flux control (DB-DTFC)[21]. As it can be observed from (15), the inductive saliency-based self-sensing control requires a certain degree of saliency (i.e., differential inductance); the following section will present the proposed control technique to temporarily increase the machine saliency using intentional magnetic saturation.

III. SPMSM SALIENCY CHARACTERISTIC AND MAGNETIC SATURATION EFFECT AND PM FLUX

This section shows how to induce an intentional magnetic saturation to enhance HFI based self-sensing capability in low saliency machines.
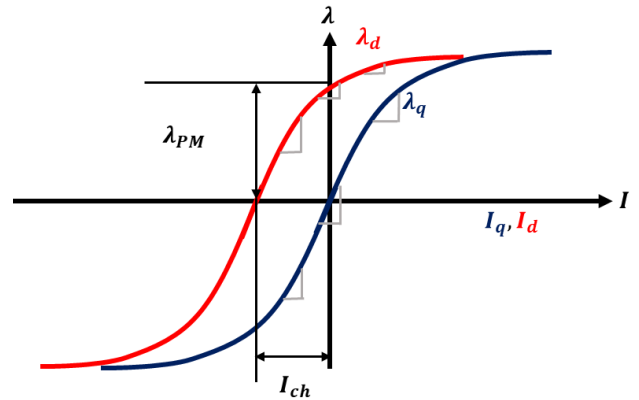

FIGURE 1. D- and q-axes flux-linkage variations with PM flux biasing d-axis vs. current.

Figure 1 shows d and q-axes flux-linkage map as a function of dq-axes currents; the d-axis flux-linkage, λ_d, in Fig. 1 being biased with the PM flux-linkage, λ_{PM}; I_{ch}, see (16), representing the characteristic current where L_d is the absolute d-axis inductance [22]. The incremental d/q-axes inductance, L_{dd}, L_{qq}, L_{qd}, and L_{dq}, respectively, are defined as the slope of the dq-axes flux-linkage at each operating point (i.e., at each d/q-axes current) (17), (18), (19), and (20) respectively. It can be observed from Fig. 1 that L_{dd} decreases if positive d-axis current is injected, i.e., flux intensifying (FI) current, while it decreases if negative d-axis current is applied, i.e., flux weakening FW current. On the other hand, L_{qq} is seen to decrease if positive/negative q-axis current is applied, symmetrical behavior being observed.

It can be concluded from Fig. 1 that although a machine is symmetrically designed, i.e., no inductive saliency exists

from the rotor geometry, e.g., SPMSM, magnetic saturation results in no-load inductive saliency; unfortunately, this saliency is typically very small [23], placing reliability concerns for HFI based self-sensing control. However, it can also be concluded from Fig. 1 that injecting d-axis FI current will increase the machine saliency; the proposed technique in this article will take advantage of this behavior to enhance HFI based self-sensing capability in low saliency machines.

$$I_{ch} = \frac{\lambda_{PM}}{L_d} \quad (16)$$

$$L_{dd} = \frac{\partial \lambda_d}{\partial i_d} \quad (17)$$

$$L_{qq} = \frac{\partial \lambda_q}{\partial i_q} \quad (18)$$
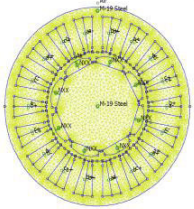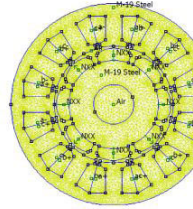
$$L_{qd} = \frac{\partial \lambda_q}{\partial i_d} \quad (19)$$

$$L_{dq} = \frac{\partial \lambda_d}{\partial i_q} \quad (20)$$

IV. SPMSM INDUCTANCE CHARACTERIZATION UNDER FI AND FW OPERATION USING FEA

This section presents the inductance characterization, FEA based, of the two SPMSMs that will be used for the experimental verification of the method: a Distributed Windings (DW) SPMSM and a Factional Slot Concentrated Windings (FSCW) SPMSM; parameters of both machines are shown in TABLE 1.

TABLE 1. Test DW and FSCW SPMSMs Parameters.

	DW SPMSM	FSCW SPMSM
Section view		
Model	*Teknic-M2310P*	*CMC-T0603P0105*
P_{rated} [W]	144	525
ω_{rated} [rpm]	5000	6790
# pole	8	8
# slot	18	12
I_{rated} [A]	7	6
R_p [Ω]	0.38	0.39
L_p [mH]	0.24	0.67
k_e [V_{pk}/(rad/sec)]	0.026	0.083
k_t [A_{pk}/Nm]	0.038	0.12

Figures 2 and 3 show the incremental inductances maps, L_{dd} and L_{qq}, including FI and FW operation regions, of the DW and FSCW SPMSMs, respectively; L_{dd} and L_{qq} being obtained as the slope of the respective flux-linkages at each operating point. As expected, L_{dd} in both SPMSMs, decreases as FI current is injected (i.e., positive d-axis current), resulting therefore in a saliency increase; the differential inductances maps being shown in Fig. 4. It can be
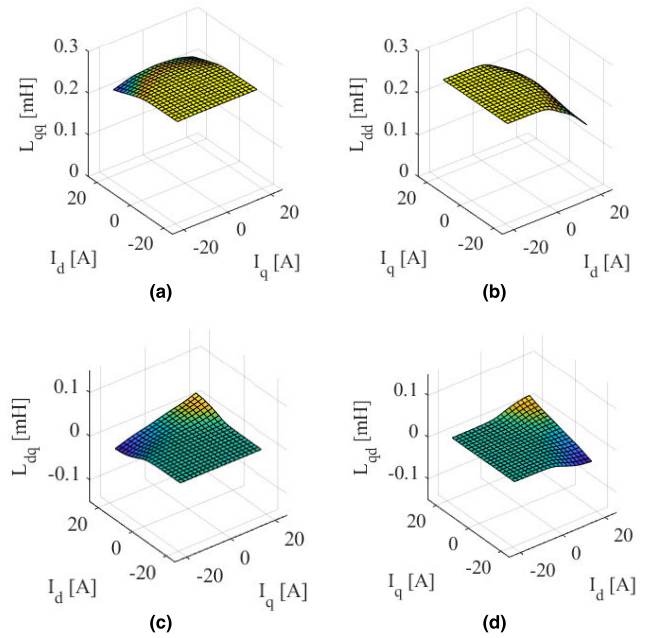

FIGURE 2. Incremental inductance map of 8-pole/18-slot DW SPMSM vs. current. (a) L_{qq}. (b) L_{dd}. (c) L_{dq}. (d) L_{qd}.
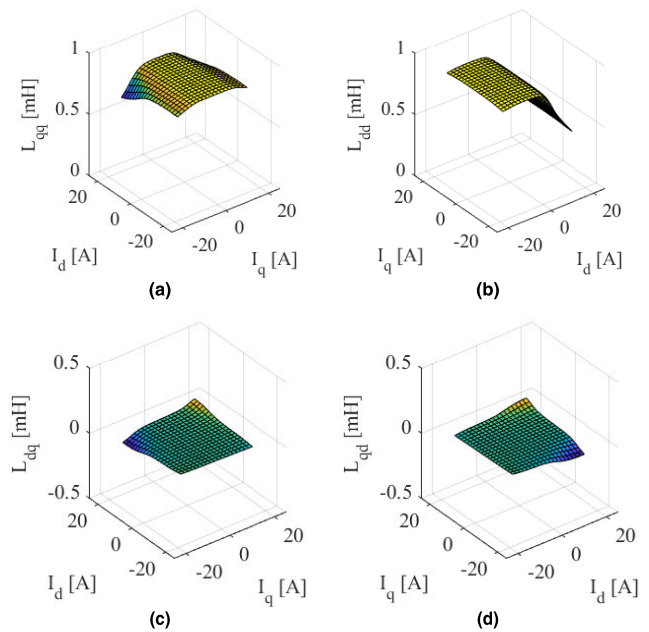

FIGURE 3. Incremental inductance map of 8-pole/12-slot FSCW SPMSM vs. current. (a) L_{qq}. (b) L_{dd}. (c) L_{dq}. (d) L_{qd}.

concluded from Figs. 2-4 that FSCW SPMSM shows higher L_{dd} variation with FI current, meaning that FSCW SPMSM has a higher ability for FI operation utilizing intentional magnetic saturation. This is expected since FSCW machines have larger inductance than DW machines [24].

It is interesting to note that SPMSMs has low cross-coupled inductances, L_{dq} and L_{qd}, which are the results of cross-saturation. This is because of the absence of flux barriers,
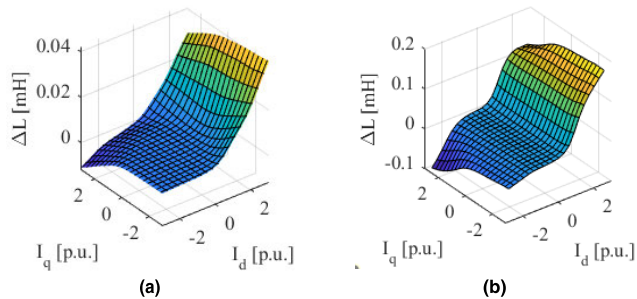
FIGURE 4. Differential inductance map with current in per unit.
(a) 8-pole/18-slot DW SPMSM. (b) 8-pole/12-slot FSCW SPMSM.

which are typically included in IPMSMs to increase reluctance torque production, and can be highly cross-saturated under loaded operation [25]. In addition, the equivalent airgap in SPMSMs is larger than in IPMSM due to the surface-mounted PMs, which makes the rotor iron saturation level to be lesser affected by the stator currents than in IPMSMs. For these reasons, the HFI model of SPMSMs can be simplified to (1), where the cross-coupled inductances are merged to main-inductance. Even more, all these issues pointed out that the optimal HF injection angle in SPMSMs is 0 deg., i.e., d-axis pulsating HF signal injection.

V. IMPLEMENTATION OF FI HFI SELF-SENSING

In this section, the control block diagram of HFI based self-sensing using FI current injection is presented. The proposed implementation includes also PM polarity estimation and the tradeoff of the proposed self-sensing technique in the additional power.
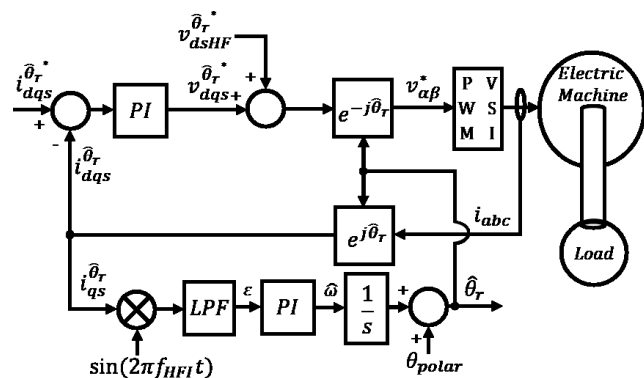

FIGURE 5. Closed-loop self-sensing control block diagram with field-oriented control, including the injection of the HF signal and position estimation.

A. CONTROL BLOCK DIAGRAM OF HFI BASED SELF-SENSING AND FI CURRENT

Figure 5 shows the control block diagram of classical HFI based self-sensing based filed-oriented control (FOC) in the estimated rotor reference frame. The HF pulsating voltage in (6) can result in HF current in the orthogonal axis as in (13) when reference frame error exists. Positive d-axis

current is commanded for FI operation in zero-to-low speed self-sensing using intentional magnetic saturation, creating required inductive saliency on SPMSMs with small saliency.

$$i_d = \frac{V_{HFI}\sin(\theta_{HFI})}{2\omega_{HFI}L_{dd}\{i_d\}} \qquad (21)$$

B. PM POLARITY DETECTION

PM polarity is detected using secondary saliency induced on the d-axis by the magnetic saturation effect [26], [27]. The initial inductive saliency, although small typically $<5\sim10\%$, can be used to find the d-axis by using the HFI self-sensing technique shown in Section II [1]; the magnet polarity can be detected using the secondary harmonic HF current component induced by saturation effect [26], [27].
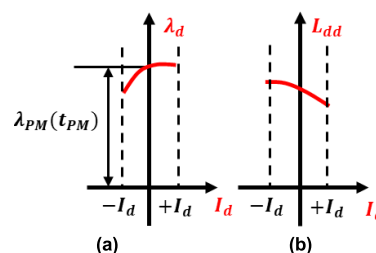

FIGURE 6. (a) D-axis flux-linkage, λ_d. (b) D-axis incremental inductance, Ldd, with positive and negative d-axis current, I_d.

The left and the right figure in Fig. 6 show the d-axis flux-linkage map and d-axis incremental inductance near zero d-axis current, respectively. The resulting d-axis incremental inductance, L_{dd}, decreases when the pulsating current is in the FI region; L_{dd} increases in FW region. It can be observed from (21) that the d-axis HF current will change inversely proportional to L_{dd}. Figure 7 shows the d-axis current response with saturation induced secondary harmonic component, i_{d2}, the first order harmonic current, i_{d1}, and the total current response, i_d, which is the sum of i_{d1} and i_{d2}. When the north (N) pole is aligned with d-axis, the saturation induces positive secondary harmonic; the negative secondary harmonic will be induced when the south (S) pole is aligned with d-axis. By extracting the secondary harmonic component, as shown in Fig 8, PM polarity can be detected. The detection process is only required once at the starting of the SPMSMs.

C. POWER REQUIRED FOR FI HFI

The required power for FI HFI operation, $P_{FI\ HFI}$, is represented by (22).

$$P_{FIHFI} = P_{HFI} + P_{FI} \qquad (22)$$

As it can be observed, P_{FIHFI} is composed of two terms:

- P_{FI}: required power to operate a machine in the FI region, i.e., additional power due to positive d-axis current injection (23); where R_p is the rated phase resistance. Figure 9 shows measured and estimated (using (23)) P_{FI}. As expected, P_{FI} increases as the
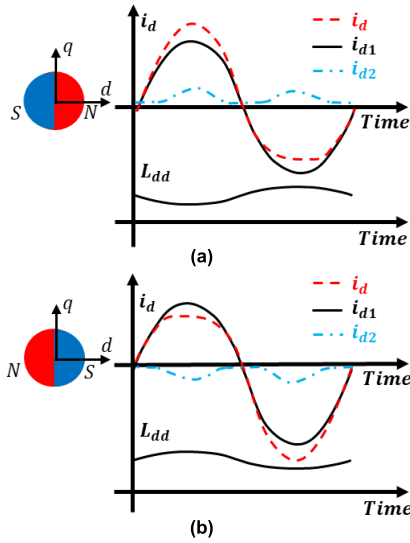
FIGURE 7. HF current response including fundamental and secondary current. (a) N-pole aligned with d-axis. (b) S-pole aligned with d-axis.
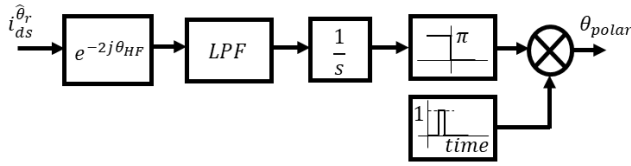

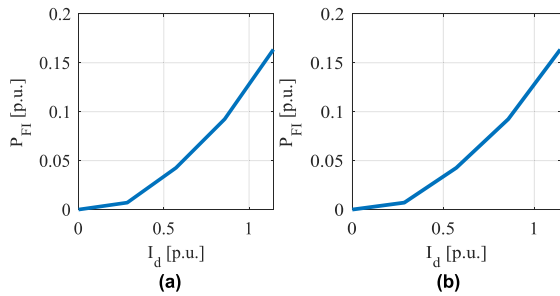**FIGURE 8.** PM polarity detection post-processing block diagram.

FIGURE 9. FI operation loss, P_{FI} with d-axis current in per unit, P_{rated} = 144W. (a) Measured P_{FI}. (b) Estimated P_{FI}.

d-axis current does. It is noted that this additional power required for intentional magnetic saturation will be required only temporarily when zero-to-low speed self-sensing is required. At medium-to-high speed operation region, where trackable back-EMF exists, back-EMF based self-sensing method can be used, d-axis current can be therefore controlled to be zero.

$$P_{FI} = \frac{3}{2}I_d^2 R_p \qquad (23)$$

- P_{HFI}: required power to inject the HF signal (24) where L_p is rated phase inductance, and V_{HFI} and f_{HFI} are the magnitude and frequency of the injected HF signal. Figure 10 shows the measured and estimated (using (24)) P_{HFI} as a function of V_{HFI} and ω_{HFI}. It can
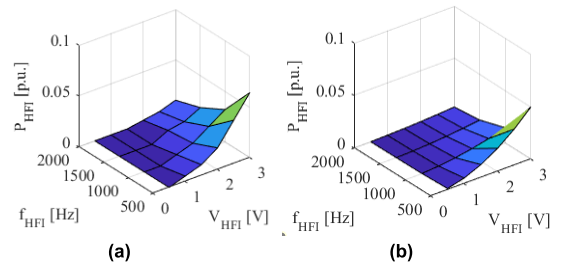

FIGURE 10. HF injection loss, P_{HFI} with varying V_{HFI} and f_{HFI}, P_{rated} = 144W. (a) Measured P_{HFI}. (b) Estimated P_{HFI}.

be observed that the higher the frequency of the HF signal, the lower the losses, and, as expected, the lower the magnitude of the HF signal, the lower the losses.

$$P_{HFI} = \frac{3}{2}R_p \frac{V_{HFI}^2}{R_p^2 + (\omega_{HFI}L_p)^2} \qquad (24)$$

VI. EXPERIMENTAL RESULTS

This section provides experimental to demonstrate the viability of the proposed technique. Figure 11 shows the experimental setup, which consists of an XCS2000 controller, DRV8301 inverters with 20kHz switching frequency, and back-to-back connected SPMSMs (load and test machines).
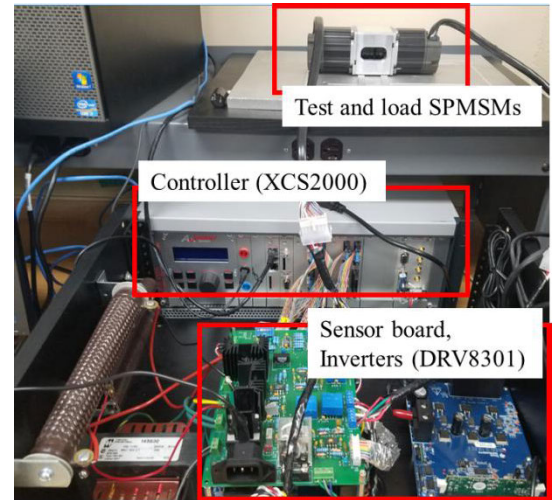

FIGURE 11. Experimental setup: test and load SPMSMs, controller (XCS2000), sensor board, and inverters (DRV8301).

A. NO LOAD INDUCANCE ESTIMATION D

and q-axes incremental inductances, L_{dd} and L_{qq}, have been measured in both test machines (DW and FSCW SPMSMs); L_{dd} and L_{qq} being obtained form (25).

The procedure to measure L_{dd} and L_{qq} is the following:
1. Phase-to-phase inductance, L_{uv} (25), is measured using an RLC meter while the rotor of the machine is positioned at $\pi/3$ and $5\pi/6$; two frequencies for the HF signal have been used 10^2 and 10^3 Hz.

2. L_{dd} and L_{qq} are obtained from the measurements provided by the RLC meter as (26) and (27).

$$L_{uv}(\theta_e) = L_{qq} + L_{dd} + (L_{qq} - L_{dd})\cos\left(2\theta_e + \frac{\pi}{3}\right)$$
(25)

$$L_{dd} = \frac{L_{uv}\left(\frac{\pi}{3}\right)}{2}$$
(26)

$$L_{qq} = \frac{L_{uv}\left(\frac{5\pi}{6}\right)}{2}$$
(27)

The results are summarized in TABLE 2. It can be observed from TABLE 2 that the no-load inductive saliency for both machines is $\approx 10\%$. It can also be observed that the inductances decrease as the frequency of the HF signal increases; this is because skin effect on a coil tends to make resistance higher, and the skin effect on the lamination makes inductance lower. The inductance drop with frequency can be therefore explained from the decreasing effective axial direction area of lamination [28]. Nevertheless, the inductance drop due to skin effect will not affect the inductive saliency ratio since the effect exists in both dq-axes.

TABLE 2. DQ Incremental Inductance.

f_{HFI} [Hz]	DW SPMSM		CW SPMSM	
	L_{qq} [mH]	L_{dd} [mH]	L_{qq} [mH]	L_{dd} [mH]
10^2	0.263	0.222	0.795	0.755
10^3	0.216	0.197	0.575	0.530

B. INDUCTIVE SALIENCY VARIATION DUE TO FI CURRENT INJECTION

To measure the influence of soft-iron saturation effects on inductance, the dq-axes flux-linkage is estimated at the standstill position [29], [30]. At a locked rotor position, back-EMF does not exist; therefore, flux-linkage in dq-axes can be measured using (28)-(29). Dq-inductances can be estimated from (17)-(18) after applying a low-frequency square wave voltage to the machine. Figure 12 shows the inductance variation as a function of dq-current; it is observed a sharper d-axis inductance drop with positive I_d current on the FSCW SPMSM than on the DW SPMSM.

$$\lambda_q(t) = \int (v_q(\tau) - R_p i_q(\tau)) d\tau$$
(28)

$$\lambda_d(t) = \int (v_d(\tau) - R_p i_d(\tau)) d\tau$$
(29)

Figure 13 shows I_{i1} vs. fundamental d-axis current for FSCW and DW SPMSMs measured directly using high-frequency voltage injection in between dq-axes given the rotor position from the encoder [18]. Choosing $(\theta_r - \hat{\theta}_r) = 45$ [deg.] in (14), I_{i1} in (15) is estimated given the encoder position as the reference. As expected, the I_{i1} increases if the positive d-axis current is injected, FI current, and decreases if negative d-axis current is injected, FW current.
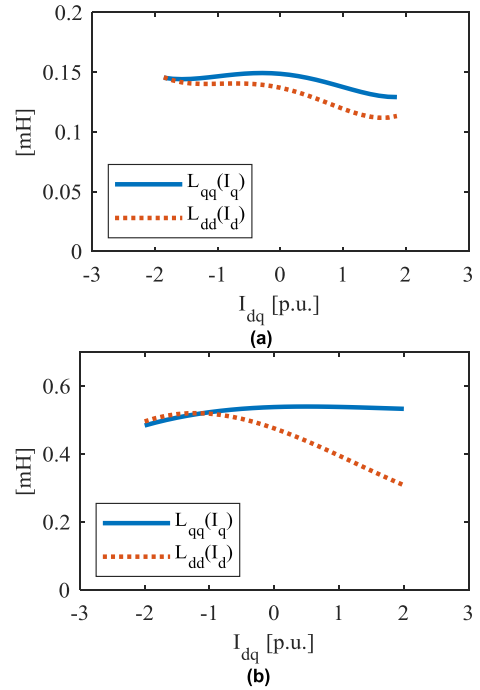

FIGURE 12. Inductance variation as function of dq-current. (a) DW SPMSM - M2310. (b) FSCW SPMSM - T0601., see TABLE 1. Square $v_{dq} = 9V$ at 10Hz $\theta_r = 0$deg.
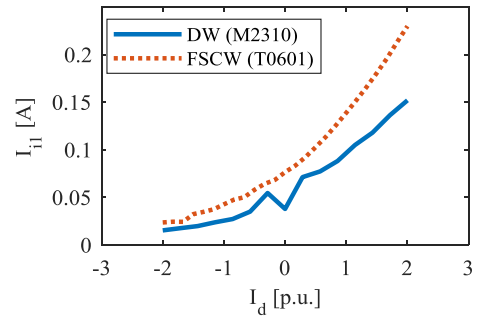

FIGURE 13. Experimental results of I_{i1} of FSCW and DW SPMSMs (see TABLE 1) in I_d range of 2p.u. with HFI $f_{HFI} = 1000$Hz, and $V_{HFI} = 2V$.

C. CLOSED LOOP FI SELF-SENSING CONTROL EXPERIMENTAL RESULTS

Figure 14 shows the command tracking ability of the conventional HFI based self-sensing position control, i.e., without FI current injection, while Fig. 15 shows the command tracking ability of the proposed HFI based self-sensing position control, i.e., with FI current injection. In both cases, see Fig. 14 (a) and 15 (a), a swept sine $i_{qsi}^{\ddagger}$ command from 0 to 20Hz was applied to the test machine. Figure 14 (b) and 15 (b) show the high-frequency injection angle error, ε see Fig. 5 (b). Figure 14 (c) and 15 (c) show the estimated position and the measured position of the conventional HFI based self-sensing position control and the proposed technique, respectively, while Fig. 14 (d) and 15 (d) show the position error, i.e., the difference between the
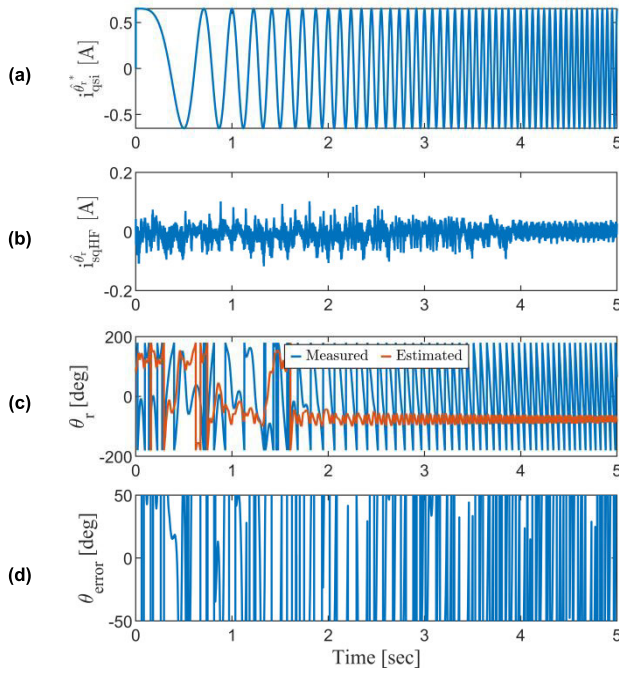
FIGURE 14. Command tracking performance of closed-loop flux-intensifying HFI self-sensing control. (a) Q-axis current command, chirp iq from 0-20Hz in 5sec. (b) LPF q-axis HF current. (c) Estimated and measured (using an encoder) rotor position. (d) Estimated position error. V_{HFI} = 3V and f_{HFI} = 1000Hz, I_d = 0A, current loop bandwidth of 500Hz, DW SPMSM - M2310, see Table 1.
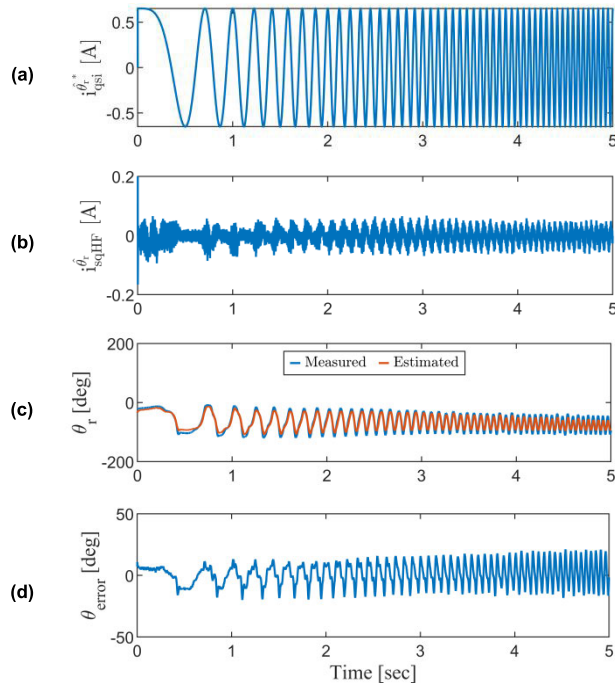
FIGURE 15. Command tracking performance of closed-loop flux-intensifying HFI self-sensing control. (a) Q-axis current command, chirp iq from 0-20Hz in 5sec. (b) LPF q-axis HF current. (c) Estimated and measured (using an encoder) rotor position. (d) Estimated position error. V_{HFI} = 3V and f_{HFI} = 1000Hz, I_d = 0.5p.u., current loop bandwidth of 500Hz, DW SPMSM - M2310, see TABLE 1.

measured and estimated position. It can be clearly observed that the proposed FI operation technique enhances the self-sensing ability.

VII. CONCLUSION

This article proposes injecting FI current to intentionally increase the inductive saliency of a PMSM, making reliable use of HFI self-sensing in machines with very low saliency, e.g., SPMSMs. It has been shown that low saliency machines became a better self-sensor under FI operation with positive d-axis current injection; injecting FI current will decrease d-axis inductance, which results in an increase of the inductive saliency required for HFI self-sensing. It has been demonstrated that by using the proposed method, neither machine design nor pre-characterization for current path planning is required for using HFI self-sensing techniques in low saliency machines. Experimental results have been provided to demonstrate the viability of the proposed technique.

ACKNOWLEDGMENT

REFERENCES

[1] M. J. Corley and R. D. Lorenz, "Rotor position and velocity estimation for a salient-pole permanent magnet synchronous machine at standstill and high speeds," *IEEE Trans. Ind. Appl.*, vol. 34, no. 4, pp. 784–789, Jul. 1998.

[2] R. M. K. Hammel, Wolfgang, "Position sensorless control of PMSM by synchronous injection and demodulation of alternating carrier voltage," in *Proc. 1st Symp. Sensorless Control Electr. Drives*, Jul. 2010, pp. 56–63.

[3] W. Hammel and R. M. Kennel, "High-resolution sensorless position estimation using delta-sigma-modulated current measurement," in *Proc. IEEE Energy Convers. Congr. Exposit.*, Sep. 2011, pp. 2717–2724.

[4] Z. Q. Zhu and L. M. Gong, "Investigation of effectiveness of sensorless operation in carrier-signal-injection-based sensorless-control methods," *IEEE Trans. Ind. Electron.*, vol. 58, no. 8, pp. 3431–3439, Aug. 2011.

[5] S.-C. Yang, T. Suzuki, R. D. Lorenz, and T. M. Jahns, "Surface-permanent-magnet synchronous machine design for saliency-tracking self-sensing position estimation at zero and low speeds," *IEEE Trans. Ind. Appl.*, vol. 47, no. 5, pp. 2103–2116, Sep. 2011.

[6] N. Bianchi, S. Bolognani, J.-H. Jang, and S.-K. Sul, "Comparison of PM motor structures and sensorless control techniques for zero-speed rotor position detection," *IEEE Trans. Power Electron.*, vol. 22, no. 6, pp. 2466–2475, Nov. 2007.

[7] H. M. Flieh, R. D. Lorenz, E. Totoki, S. Yamaguchi, and Y. Nakamura, "Investigation of different servo motor designs for servo cycle operations and loss minimizing control performance," *IEEE Trans. Ind. Appl.*, vol. 54, no. 6, pp. 5791–5801, Nov. 2018.

[8] N. Limsuwan, Y. Shibukawa, D. D. Reigosa, and R. D. Lorenz, "Novel design of flux-intensifying interior permanent magnet synchronous machine suitable for self-sensing control at very low speed and power conversion," *IEEE Trans. Ind. Appl.*, vol. 47, no. 5, pp. 2004–2012, Sep. 2011.

[9] M. Barcaro, M. Morandin, T. Pradella, N. Bianchi, and I. Furlan, "Iron saturation impact on high-frequency sensorless control of synchronous permanent-magnet motor," *IEEE Trans. Ind. Appl.*, vol. 53, no. 6, pp. 5470–5478, Nov. 2017.

[10] Y. Li, Z. Q. Zhu, D. Howe, C. M. Bingham, and D. A. Stone, "Improved rotor-position estimation by signal injection in brushless AC motors, accounting for cross-coupling magnetic saturation," *IEEE Trans. Ind. Appl.*, vol. 45, no. 5, pp. 1843–1850, Jul. 2009.

[11] J. Lee, Y. C. Kwon, and S. K. Sul, "Signal-injection sensorless control with tilted current reference for heavily saturated IPMSMs," *IEEE Trans. Power Electron.*, vol. 35, no. 11, pp. 12100–12109, Apr. 2020.

[12] T. Kojima, T. Suzuki, M. Hazeyama, and S. Kayano, "Position sensorless control of synchronous reluctance machines based on magnetic saturation depending on current phase angles," *IEEE Trans. Ind. Appl.*, vol. 56, no. 3, pp. 2171–2179, Jan. 2020.

[13] J.-H. Jang, S.-K. Sul, J.-I. Ha, K. Ide, and M. Sawamura, "Sensorless drive of surface-mounted permanent-magnet motor by high-frequency signal injection based on magnetic saliency," *IEEE Trans. Ind. Appl.*, vol. 39, no. 4, pp. 1031–1039, Jul. 2003.

[14] T. C. Lin and Z. Q. Zhu, "Sensorless operation capability of surface-mounted permanent-magnet machine based on high-frequency signal injection methods," *IEEE Trans. Ind. Appl.*, vol. 51, no. 3, pp. 2161–2171, May 2015.

[15] Z. Chen, X. Cai, R. Kennel, and F. Wang, "Enhanced sensorless control of SPMSM based on stationary reference frame high-frequency pulsating signal injection," in *Proc. IEEE 8th Int. Power Electron. Motion Control Conf. (IPEMC-ECCE Asia)*, Hefei, China, 2016, pp. 885–890, doi: 10.1109/IPEMC.2016.7512403.

[16] Y.-R. Lee, Y.-C. Kwon, and S.-K. Sul, "Realization of signal-injection sensorless control of SMPMSM by modification of current trajectory," in *Proc. IEEE Energy Convers. Congr. Expo. (ECCE)*, Oct. 2020, pp. 5117–5123.

[17] Y. G. Kang and R. D. Lorenz, "Using intentional magnetic saturation for HFI based self-sensing with SPMSMs," in *Proc. PEDES*, Dec. 2018, pp. 1–6.

[18] Y. G. Kang, D. Reigosa, B. Sarlioglu, and R. Lorenz, "D and Q-axes inductance estimation and self-sensing condition monitoring using 45 angle high-frequency injection," *IEEE Trans. Ind. Appl.*, early access, Oct. 9, 2020, doi: 10.1109/TIA.2020.3029993.

[19] M. Barcaro, M. Morandin, T. Pradella, N. Bianchi, F. Member, and I. Furlan, "Iron saturation impact on high frequency sensorless control of synchronous permanent magnets Motor," in *Proc. 22nd Int. Conf. Electr. Mach. ICEM*, vol. 53, no. 6, Sep. 2016, pp. 1085–1091.

[20] P. L. Jansen, R. D. Lorenz, and D. W. Novotny, "Observer-based direct field orientation: Analysis and comparison of alternative methods," *IEEE Trans. Ind. Appl.*, vol. 30, no. 4, pp. 945–953, Jul. 1994.

[21] J. S. Lee, C. H. Choi, J. K. Seok, and R. D. Lorenz, "Deadbeat-direct torque and flux control of interior permanent magnet synchronous machines with discrete time stator current and stator flux-linkage observer," *IEEE Trans. Ind. Appl.*, vol. 47, no. 4, pp. 1749–1758, May 2011.

[22] T. M. Jahns, "Flux-weakening regime operation of an interior permanent-magnet synchronous motor drive," *IEEE Trans. Ind. Appl.*, vol. IA-23, no. 4, pp. 681–689, Jul. 1987.

[23] W. L. Soong, "Field-weakening performance of brushless synchronous AC motor drives," *IEE Proc. Electr. Power Appl.*, vol. 141, no. 6, p. 331, Nov. 1994.

[24] A. M. El-Refaie and T. M. Jahns, "Optimal flux weakening in surface PM machines using fractional-slot concentrated windings," *IEEE Trans. Ind. Appl.*, vol. 41, no. 3, pp. 790–800, May/Jun. 2005.

[25] P. Sergeant, F. De Belie, and J. Melkebeek, "Rotor geometry design of interior PMSMs with and without flux barriers for more accurate sensorless control," *IEEE Trans. Ind. Electron.*, vol. 59, no. 6, pp. 2457–2465, Jun. 2012.

[26] D. Raca, P. Garcia, D. D. Reigosa, F. Briz, and R. D. Lorenz, "Carrier-Signal Selection for Sensorless Control of PM Synchronous Machines at Zero and Very Low Speeds," *IEEE Trans. Ind. Appl.*, vol. 46, no. 1, pp. 167–178, Jan. 2010.

[27] Y.-S. Jeong, R. D. Lorenz, T. M. Jahns, and S.-K. Sul, "Initial rotor position estimation of an interior permanent-magnet synchronous machine using carrier-frequency injection methods," *IEEE Trans. Ind. Appl.*, vol. 41, no. 1, pp. 38–45, Jan. 2005.

[28] S. Ovrebo, R. Nilssen, and R. Nilsen, "High frequency flux distribution in permanent magnet synchronous machines," in *Proc. Norpie Conf.*, no. 1, Jul. 2004, pp. 2–7.

[29] B. Stumberger, G. Stumberger, D. Dolinar, A. Hamler, and M. Trlep, "Evaluation of saturation and cross-magnetization effects in interior permanent-magnet," *IEEE Trans. Ind. Appl.*, vol. 39, no. 5, pp. 1264–1271, Sep. 2003.

[30] Y. Gao, R. Qu, Y. Chen, J. Li, and W. Xu, "Review of off–line synchronous inductance measurement method for permanent magnet synchronous machines," in *Proc. IEEE Conf. Expo Transp. Electrif. Asia–Pacific (ITEC Asia–Pacific)*, Aug. 2014, pp. 1–6.

YE GU KANG (Member, IEEE) received the B.S. degree in electrical engineering from Penn State University, University Park, PA, USA, in 2011, and the M.S. degree in electrical engineering and the Ph.D. degree in mechanical engineering from the University of Wisconsin–Madison, Madison, WI, USA, in 2013 and 2019, respectively. He is currently an Investigator with the University of Oviedo, Gijon, Spain. His research interest includes the design and control of energy conversion devices.

DAVID DIAZ REIGOSA (Member, IEEE) was born in Spain 1979. He received the M.E. and Ph.D. degrees in electrical engineering from the University of Oviedo, in 2003 and 2007, respectively. From 2004 to 2008, he was awarded and fellowship of the Personnel Research Training Program funded by the Regional Ministry of Education and Science of the Principality of Asturias. He was a Visitor Scholar with the Wisconsin Electric Machines and Power Electronics Consortium, University of Wisconsin–Madison, Madison, in 2007. He was a Visitor Professor with the Electrical Machines and Drives Group, University of Sheffield, U.K., in 2016. He is currently an Associate Professor with the Electrical Engineering Department, University of Oviedo. His research interests include the sensorless control of induction motors, permanent magnet synchronous motors, and digital signal processing. He was a recipient of nine IEEE Industry Applications Society Conference and the IEEE Energy Conversion Congress and Exposition prize paper awards.

ROBERT D. LORENZ (Life Fellow, IEEE) received the B.S.M.E. and M.S.M.E. degrees in controls from the University of Wisconsin–Madison, Madison, WI, USA, in 1969 and 1970, respectively, the M.B.A. degree from the University of Rochester, Rochester, NY, USA, in 1980, and the Ph.D. (M.E.) degree in controls from the University of Wisconsin–Madison, in 1984. From 1984, he was a Faculty Member with the Department of Mechanical Engineering, University of Wisconsin–Madison, and also an Associate Director of the Wisconsin Electric Machines and Power Electronics Consortium (WEMPEC). He was with industry for 12 years, working on high-performance drives and synchronized motion control. From 1997 to 2019, he was the Co-Director of WEMPEC. He has authored more than 400 technical articles and has more than 45 patent awards and applications in his research topics. His research interests include power electronics, drives, self-sensing, current regulators, and motion control.

Dr. Lorenz was a recipient of several awards from the IEEE Industry Applications Society and the European Power Electronics Associations, the 2014 IEEE Richard H. Kaufman Technical Field Award, and the 33 IEEE Prize Paper Awards. He was the IEEE Division II Director, from 2005 to 2006, IEEE IAS President, in 2001, and a Distinguished Lecturer of IAS, from 2000 to 2001. He was posthumously elected to the U.S. National Academy of Engineering, in 2019.

● ● ●